

TRGB DISTANCES TO GALAXIES IN FRONT OF THE VIRGO CLUSTER

IGOR D. KARACHENTSEV,¹ LIDIA N. MAKAROVA,¹ R. BRENT TULLY,² LUCA RIZZI,³ AND
EDWARD J. SHAYA⁴

¹*Special Astrophysical Observatory, Nizhniy Arkhyz, Karachai-Cherkessia 369167, Russia*

²*Institute for Astronomy, University of Hawaii, 2680 Woodlawn Drive, HI 96822, USA*

³*W. M. Keck Observatory, 65-1120 Mamalahoa Hwy, Kamuela, HI 96743, USA*

⁴*Astronomy Department, University of Maryland, College Park, MD 20743, USA*

Submitted to ApJ

ABSTRACT

Tip of the red giant branch distances are acquired from Hubble Space Telescope images for 16 galaxies to the foreground of the Virgo Cluster. The new distances with 5% accuracy, combined with archival measurements, tightly constrain the near side location of the onset of infall into the Virgo Cluster to be 7.3 ± 0.3 Mpc from the cluster, reaching within 9 Mpc of the Milky Way. The mass within this turnaround radius about the cluster is $8.3 \pm 0.9 \times 10^{14} M_{\odot}$. Color-magnitude diagrams are provided for galaxies in the study and there is brief discussion of their group affiliations.

Keywords: galaxies: distances and redshifts — galaxies: dwarf — galaxies: stellar content

1. INTRODUCTION

The nearest galaxies lie in a flattened structure on the supergalactic equator that we have called the Local Sheet (Tully et al. 2008). The Local Sheet is a wall of the Local Void that occupies most of the nearby volume above the supergalactic equator (positive SGZ). The Virgo Cluster lies within the supergalactic equatorial band beyond the Local Sheet at 16 Mpc.

Over the years, imaging with Hubble Space Telescope (HST) has led to estimates of the distances to nearby galaxies from the measured luminosities of the brightest resolved red giant branch stars: the so-called tip of the red giant branch (TRGB) method. These observations have culminated in two HST-SNAP programs which gave, for any galaxy within 10 Mpc, a distance accurate to 5% with a single HST orbit. There are now almost 400 accurate TRGB distances in the Local Volume Galaxy Database (<http://www.sao.ru/lv/lvgdb/>) and Extragalactic Distance Database (EDD) (<http://edd.ifa.hawaii.edu/>). The morphology and kinematics of nearby structure is becoming increasingly clarified. On a very local scale (<5 Mpc) we now have a detailed knowledge of the nature of galaxy groups: their memberships, dimensions, velocity dispersions, and infall patterns (Karachentsev 2005; Tully 2015; Kashibadze & Karachentsev 2018; Shaya et al. 2017). Associations of dwarfs probe the clustering regime at the halo level of $10^{11}M_{\odot}$ (Tully et al. 2006). The curious phenomenon of satellite layering is being documented (Ibata et al. 2013; Shaya & Tully 2013; Tully et al. 2015).

There are gaps between the Local Sheet and neighboring structure. The galaxies within the Local Sheet are found to be moving coherently, with minimal dispersion. The distances to galaxies within the Local Sheet are very close to expectations from the Hubble flow (Karachentsev et al. 2009). By contrast, nearby galaxies off the supergalactic equator essentially all have substantial negative velocities compared to Hubble law expectations. The structures below the plane that are accessible to TRGB measurements were given the names Leo Spur and Dorado Cloud in the Nearby Galaxies Atlas (Tully & Fisher 1987). There is a clear velocity discontinuity between the Local Sheet and these structures. The discontinuity is explained by a bulk motion of the Local Sheet toward negative SGZ of 260 km s^{-1} due to the expansion of the Local Void (Tully et al. 2008; Karachentsev et al. 2015a), a motion not experienced by the filaments at lower SGZ. In the opposite direction toward

positive SGZ there are few galaxies and only two in the Local Void with TRGB distances: KK246 and ALFAZOAJ1952+1428 (Rizzi et al. 2017). Both these objects have large peculiar velocities toward the Local Sheet and away from the void center.

In addition to the motion away from the Local Void, members of the Local Sheet are moving together toward the Virgo Cluster, roughly in the positive SGY direction, at 185 km s^{-1} (Aaronsen et al. 1982; Tully et al. 2008).

This increasingly detailed knowledge of our local region speaks to the success of the HST-SNAP programs. However, the SNAP approach has reached a limitation. Most galaxies within 10 Mpc, the limit of the TRGB capability with single orbit HST observations, lie close to the supergalactic equator, indeed, in the Local Sheet, and pile up in a narrow Right Ascension window around 12 hours. The SNAP programs have led to coverage of a high fraction of available targets around the sky except in the RA = 12 - 13 hours window. There has been a poor understanding of the nature of structure and kinematics of the Local Sheet in a swath of sky between the Canes Venatici II region and the Sombrero galaxy in the distance range 5-10 Mpc. While most galaxies within 4 Mpc have established TRGB distances, most galaxies in the Local Sheet that are suspected to lie in the interval 4-8 Mpc have not had accurately known distances.

This region is particularly interesting, because it borders the Virgo Cluster infall domain. In the spherical approximation, it has been estimated that the cluster turnaround radius separating infall from expansion lies 7.2 ± 0.7 Mpc from the Virgo core (Karachentsev et al. 2014). The front edge of this surface lies 9 Mpc from us. The volume that the Lambda-CDM model predicts will ultimately collapse into the Virgo Cluster (Peirani & de Freitas Pacheco 2008) extends to within 6 Mpc of our location. In this radial domain the density of galaxies associated with the Local Sheet falls off rapidly. Galaxies toward the far edge of the Local Sheet toward Virgo have increasingly high peculiar velocities away from us. Evidently, the attraction of the Virgo Cluster is creating a velocity shear pattern.

Our proximity to the Virgo Cluster gives us a singular opportunity to study cluster infall, which carries information about the cluster mass distribution to much larger radii than most other measures

(only weak lensing statistically explores comparable scales (Mandelbaum et al. 2006; van Uitert et al. 2011; Bahcall & Kulier 2014; Ziparo et al. 2016)). A plot from the Karachentsev et al. (2014) Virgo infall study shows that deviations from cosmic expansion evidently start to become substantial beyond 5 Mpc. Of course, the dynamics are in the non-linear regime but amenable to modeling in the spherical approximation. Shaya et al. (2017) show that the mass determined when using the spherical approximation is quite accurate at this turnaround radius despite the components of non-radial flow. A more rigorous analysis will be carried out that include all of these new high accuracy galaxy measurements with numerical action methods (Peebles 1989; Shaya et al. 1995; Peebles et al. 2001; Shaya & Tully 2013; Shaya et al. 2017) in a future study. The methodology is particularly well suited to the Virgo infall problem because, although the relationship between gravity and velocity is non-linear, the orbits have not reached shell-crossing so have only modest curvature.

In this work we present distances via the optical TRGB method for 16 galaxies in front of the Virgo Cluster using their imaging from HST. In Section 2 we outline selection of targets, results of stellar photometry, determination of galaxy distances, and summarize some individual properties of the galaxies. In Section 3 we use the new accurate distances, combined with radial velocities from NED (<http://ned.ipac.caltech.edu>) and additional distances from EDD, to constrain the near-side of the Virgo cluster infall. Two approaches are applied to estimate the uncertainty due to not knowing the true 3D motion of galaxies. As a result, we tightly constrain the near side location of the infall zone around the Virgo Cluster and estimate its total mass within the turnaround radius. Finally, in Section 4 we draw our conclusions and give a brief outlook.

2. HST/ACS OBSERVATIONS

2.1. Selection of targets

Figure 1 presents a $SGB = \pm 10^\circ$ thick and $SGL = \pm 40^\circ$ wide wedge of the Local Sheet centered on M87 ($SGB = -2.35^\circ$, $SGL = 102.88^\circ$) as the Virgo Cluster center. The Milky Way is at the origin. Galaxies with accurate TRGB or Cepheid distances are shown by solid circles and other cases with typically 20-25 per cent errors are indicated by black dots. The dotted ring identifies the projected

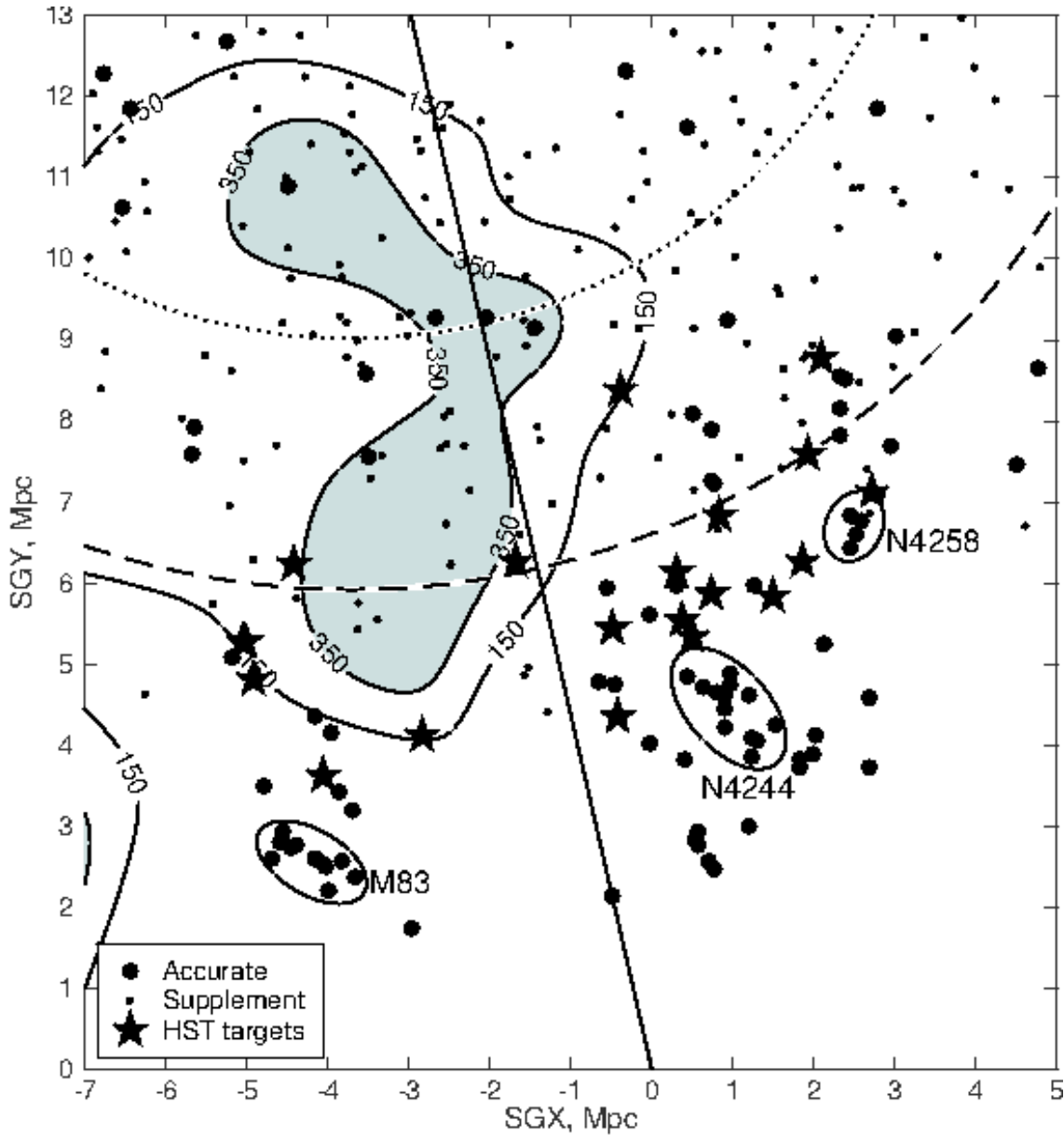


Figure 1. Distribution of galaxies in front of Virgo Cluster in Cartesian supergalactic coordinates. Solid circles and black dots are galaxies with accurate and supplement distances, respectively. The target objects are shown by asterisks. The dotted and dashed large circles correspond to the zero-velocity and zero-energy surface respectively. The region of high positive peculiar velocities is shown in gray.

zero velocity surface separating infall from cosmic expansion around the Virgo Cluster ($SGX = -3.7$ Mpc, $SGY = 16.1$ Mpc) in the spherical approximation. The straight line shows the direction toward M87. The dashed circle corresponds roughly to the zero energy surface, the outer extreme of the region that will ultimately fall into the Virgo Cluster assuming the current LCDM paradigm. Positions of

three nearby groups: M 83, NGC 4244 and NGC 4258 are marked. The gray area and the solid curve indicate a zone of positive peculiar velocities $V_{pec} = V_{LG} - 73D_{Mpc} > 350 \text{ km s}^{-1}$ and $V_{pec} = 150 \text{ km s}^{-1}$ after smoothing by a Gaussian filter with a window of 0.75 Mpc. There is an evident flow toward the Virgo Cluster. The asterisks identify 20 targets for our program of TRGB distance measurements at distances assigned from redshifts, Tully-Fisher relation and other secondary indicators. The objects are situated within $SGB = \pm 10^\circ$ and $SGL = \pm 40^\circ$ with respect to M87. Their expected distances lie in the range of 5-9 Mpc.

A list of targets is given in Table 1, where the columns contain: (1,2) galaxy name and its number in HyperLEDA (Makarov et al. 2014), (3,4) equatorial (J2000) and supergalactic coordinates, (5) total B-magnitude, (6) morphological type in numerical code according to de Vaucouleurs et al. (1991), (7) radial velocity km s^{-1} in the Local Group reference frame adopted in NASA Extragalactic Database (NED), (8,9) distance (Mpc) and the method of its estimate: from the linear Hubble flow with parameter $H_0 = 73 \text{ km s}^{-1} \text{ Mpc}^{-1}$ (h), from Tully & Fisher (1977) relation (TF), via membership in the known groups (mem); distances to two last objects: KDG218 and NGC5068 were estimated from dwarf galaxy texture (txt) and the Planetary Nebulae luminosity function (PL).

2.2. Observations and photometry

Observations of the 20 galaxies were made with the ACS/HST within the project GO-14636 (PI: I.D.Karachentsev). For each galaxy, one exposure was obtained in the F606W filter and one exposure in the F814W filter with the exposure time 1030 s in each filter. Figure 3 shows the F606W images of the galaxies. Most galaxies are well resolved into individual stars including the red giant branch (RGB).

We use the ACS module of the DOLPHOT software package¹ by A. Dolphin (Dolphin 2016) for photometry of resolved stars. The data quality images were used to mask bad pixels. Only stars of good photometric quality were used in the analysis, following the recommendations given in the DOLPHOT User's Guide. We have selected the stars with signal-to-noise (S/N) of at least five in

¹ <http://americano.dolphinim.com/dolphot/>

Table 1. List of targets for GO 14636

Name	LEDA	RA Dec	SGL SGB	B_T	T	V_{LG}	D	meth
(1)	(2)	(3)	(4)	(5)	(6)	(7)	(8)	(9)
BTS76	2832100	115844.1+273506	86.06−04.71	16.5	10	407	5.57	h
LV J1217+3231	4319966	121732.0+323157	82.75+00.77	18.2	9	433	5.93	h
LV J1218+4655	4320422	121811.1+465501	69.07+05.31	16.8	8	477	7.66	mem
KK144	166137	122527.9+282857	87.13+01.17	16.5	10	449	6.15	TF
NGC4455	041066	122844.1+224921	92.75+00.20	12.9	7	588	8.40	TF
KK151	041314	123023.8+425405	73.56+06.24	15.8	9	479	6.56	TF
UGC07678	041522	123200.4+394955	76.61+05.70	13.8	9	710	9.08	TF
KK152	041701	123324.9+332105	82.95+04.20	16.3	10	836	6.90	TF
KKSG29	042120	123714.1−102951	125.42−07.05	16.5	10	562	7.70	TF
NGC4618	042575	124132.8+410903	75.80+07.79	11.3	6	576	7.90	TF
LV J1243+4127	5056993	124355.7+412725	75.61+08.30	17.2	10	444	6.09	h
NGC4656	042863	124357.6+321013	84.68+06.02	11.0	8	635	5.40	TF
IC3840	086644	125146.1+214407	95.26+05.03	16.9	10	510	5.50	TF
UGC08061	044170	125643.4+115552	105.06+03.61	16.0	10	474	6.49	h
KK176	044681	125956.3−192447	135.49−04.04	16.5	10	618	6.90	TF
UGCA319	044982	130214.4−171415	133.54−02.94	15.1	10	555	7.30	mem
KK177	087149	130241.9+215951	95.64+07.55	17.4	−2	228	4.40	mem
DDO161	045084	130316.8−172523	133.78−02.75	13.5	8	543	7.30	TF
KDG218	045303	130544.0−074520	124.64+00.46	16.8	−1	−	5.00	txt
NGC5068	046400	131855.3−210221	138.28−00.21	10.5	6	469	5.45	PL

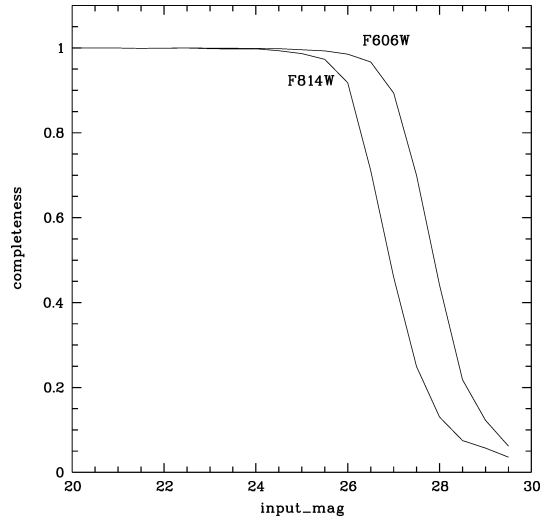


Figure 2. Photometric completeness as a function of magnitude for KK152, which is an example of fainter TRGB magnitude in our sample. As can be seen from the figure, even for this case the level of the completeness is high, and does not constrain our distance measurement.

both filters and $|sharp| \leq 0.3$. The resulting color-magnitude diagrams of the galaxies are presented in Fig. 4.

Artificial star tests provide an accurate way to estimate the photometric errors, blending and incompleteness in the crowded fields of nearby resolved galaxies. These tests were performed for the objects under study using the same DOLPHOT reduction procedures. Sufficient artificial stars were generated in the appropriate magnitude and color range so that the distribution of the recovered magnitudes is adequately sampled. Photometric errors are indicated in Fig. 4. In the CMDs we show stars with signal-to-noise ≥ 5 in both F606W and F814W filters. An example of the completeness function is given in Fig. 2 for KK152, which has one of the faintest TRGB value. As can be seen from the figure, even for this case the level of the completeness is high, and does not constrain our distance measurement. For most objects only stars located within the body of the galaxy are shown and used in further analysis. In the few cases when the galaxy is large and bright, with a significant concentration of stars in the body, we use (and show in the CMD) only the stars located in the outer, minimally obscured parts of this galaxy. These cases are indicated in the Section 2.4.

2.3. Distance determination

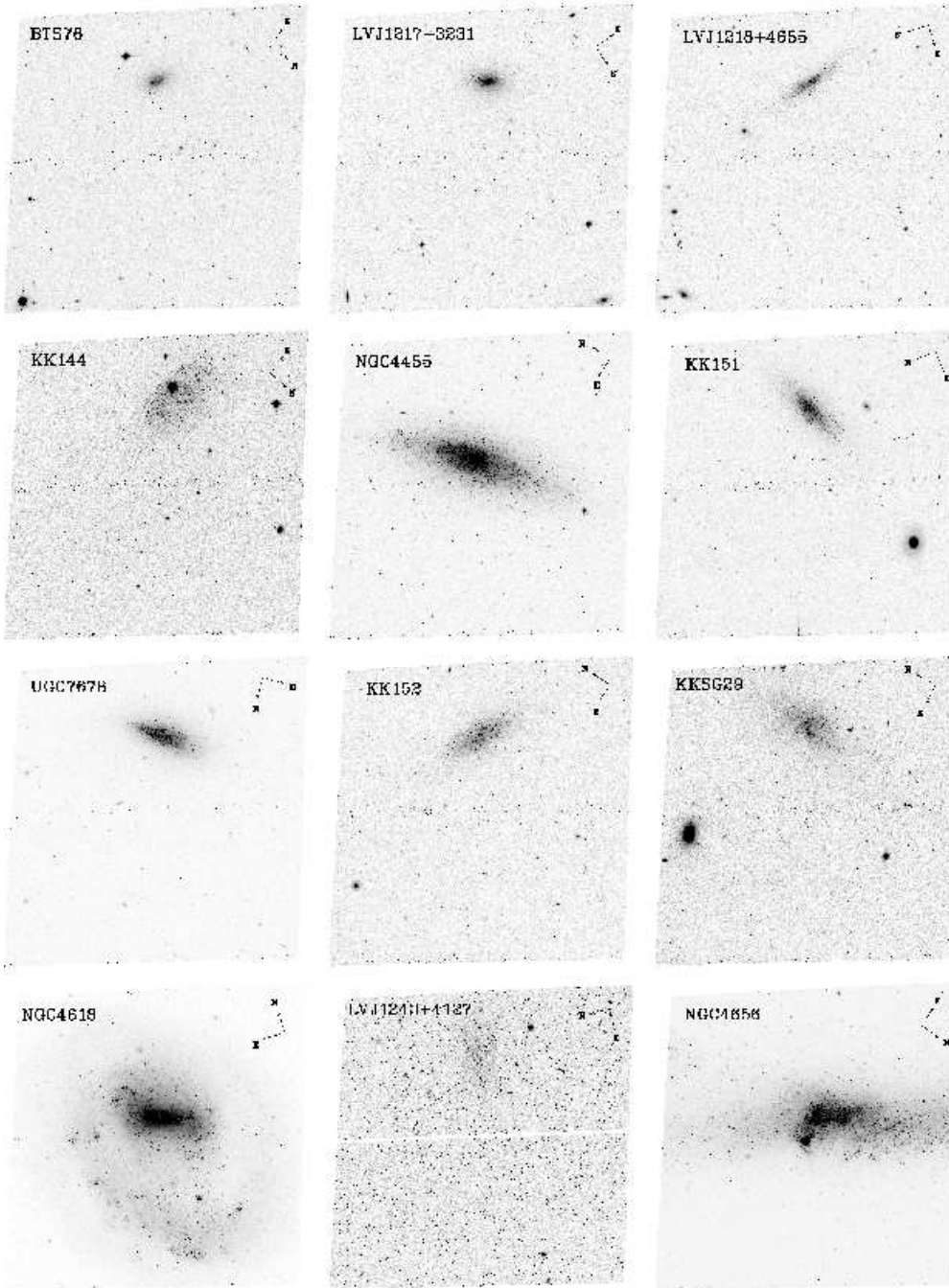


Figure 3. *HST*/*ACS* combined distortion-corrected mosaic image of the target galaxies in the *F606W* filter. The image size is 3.4×3.4 arcmin.

We have determined the photometric TRGB distance with our *trgbtool* program (Makarov et al. 2006). The program uses a maximum-likelihood algorithm to fit the RGB stellar luminosity function with a simple power law with a cutoff in the TRGB region plus a power law of a second slope for a

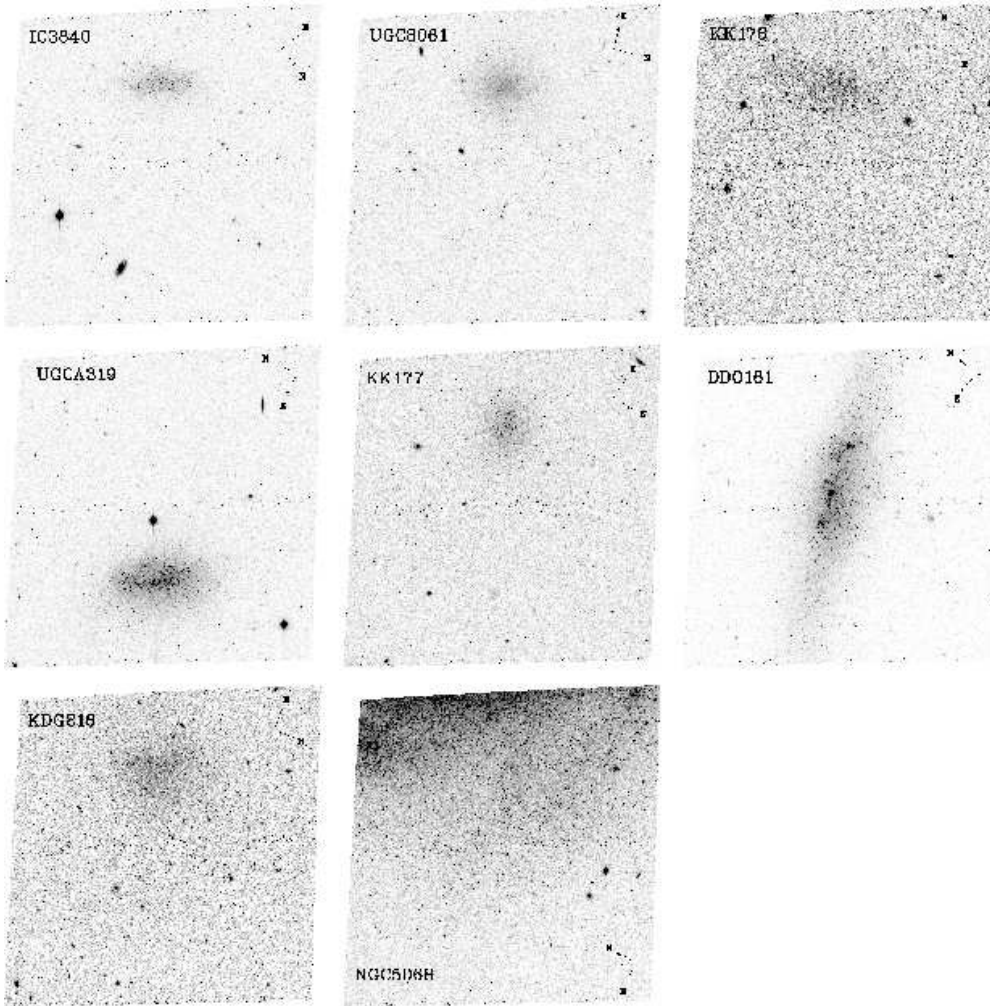


Figure 3. Continued.

stellar population brighter than the TRGB. The completeness, the photometric uncertainty, and the photometric bias are determined as a function of magnitude using artificial star experiments. They are incorporated in the maximum-likelihood fit to obtain a magnitude of TRGB. We have determined a respective $(F606W - F814W)_{TRGB}$ color using running mean over the RGB in the color-magnitude diagram of the galaxy. The measured TRGB magnitudes in the ACS instrumental system are shown in the Table 2. Using the calibration for the TRGB distance indicator by Rizzi et al. (2007) and the Galactic extinction from Schlafly & Finkbeiner (2011), we derived the true distance moduli for the program galaxies (see Table 2). The calibration of Rizzi et al. (2007) includes a zero-point and color coefficients of the transformation. The table includes: (1) galaxy name, (2) measured $F814W_{TRGB}$

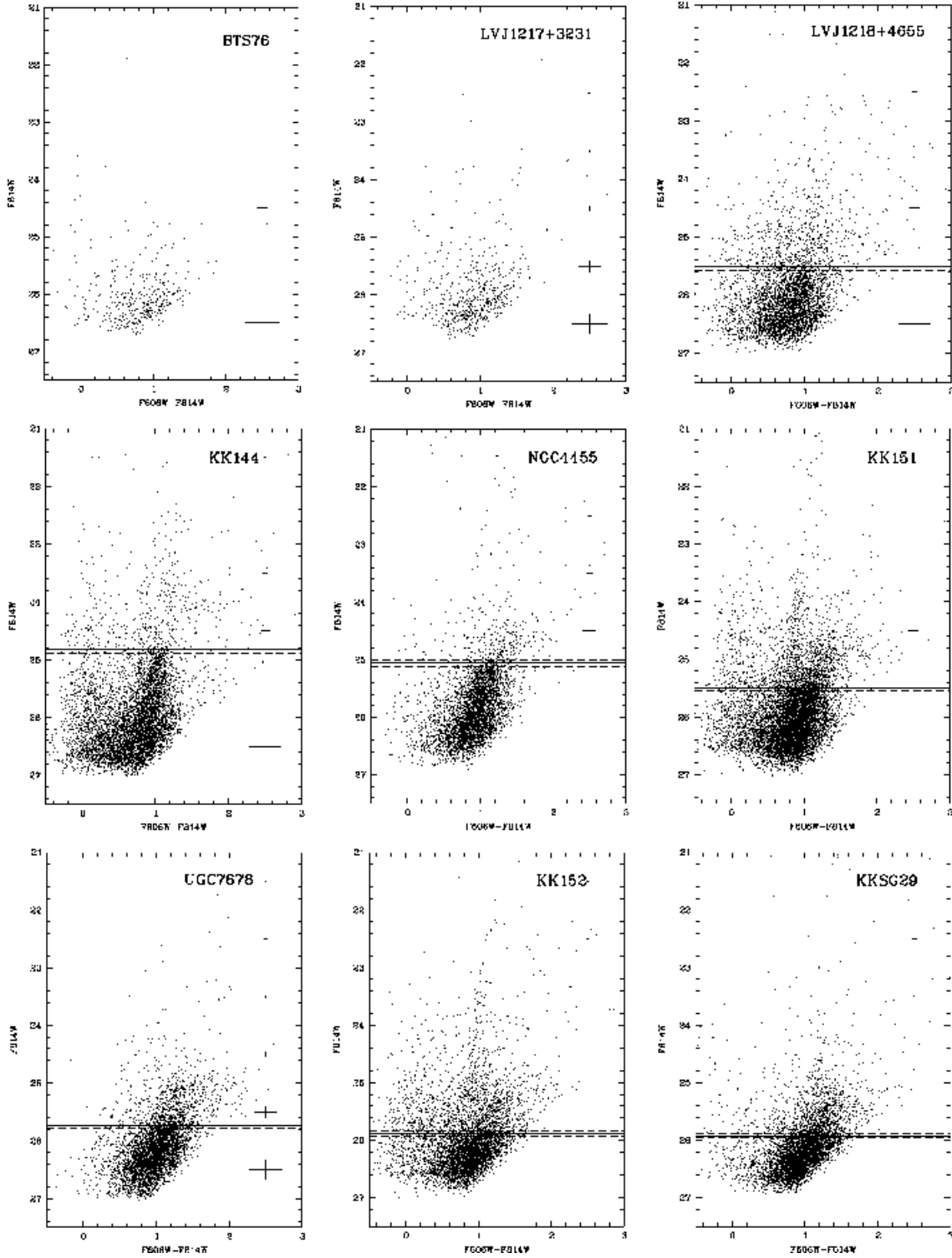


Figure 4. Color-magnitude diagrams of the target galaxies. Photometric errors are indicated by bars at the right in the CMD. Derived TRGB values are indicated with solid line, whereas the TRGB uncertainties are dashed lines.

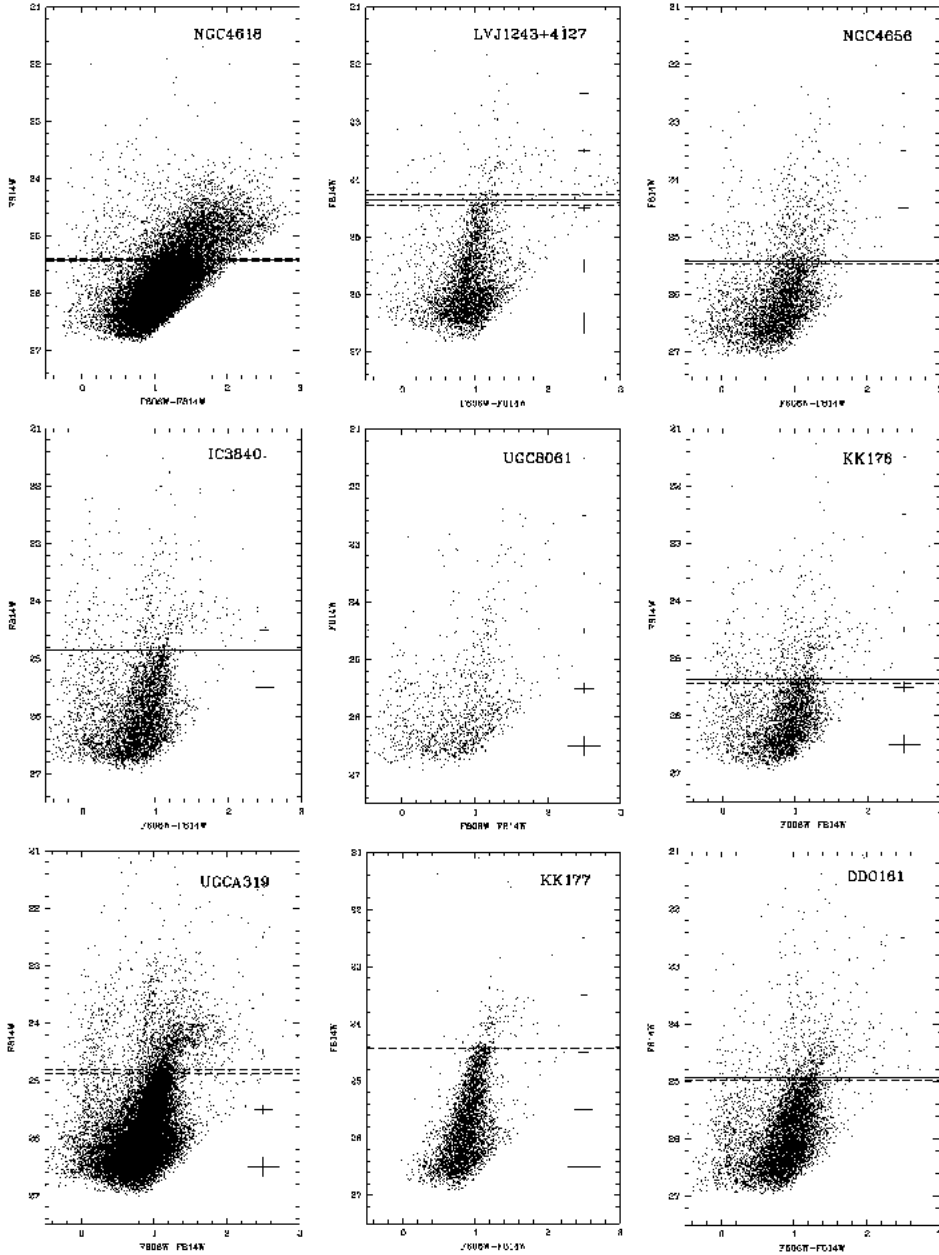


Figure 4. Continued.

value with the 68% confidence level uncertainty estimation, where photometric uncertainties are also included in the course of the maximum-likelihood fitting, (3) measured $(F606W - F814W)_{TRGB}$

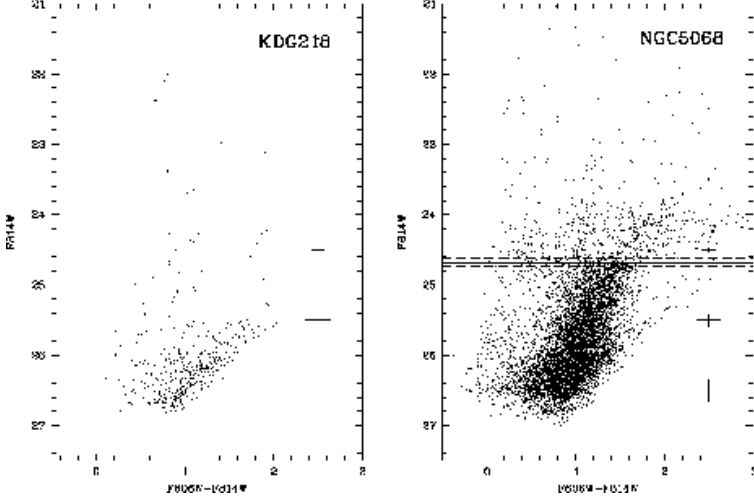


Figure 4. Continued.

value with the uncertainty, estimated from the running mean, (4) the Galactic extinction, (5) distance modulus with the uncertainty estimation, including $F814W_{TRGB}$ and $(F606W - F814W)_{TRGB}$ value uncertainties, the Galactic extinction uncertainty and the uncertainties of Rizzi et al. (2007) calibration, including the color term calibration uncertainty.

2.4. Some individual properties of the galaxies

BTS76 and LV J1217+3231. These two dwarf irregular (dIr) galaxies have radial velocities provided by the Sloan Digital Sky Survey (SDSS) (Abazajian et al. 2009). Their distances were unknown. On the images obtained with HST/ACS both galaxies are barely resolved into stars without signs of the RGB. We infer that $I_{TRGB} > 26.5$ mag and distances $D > 13$ Mpc. Judging by their low radial velocities, $V_{LG} < 500$ km s⁻¹, and distances $D > 13$ Mpc, the galaxies are related to a mysterious association of 12 to 20 galaxies projected near the E-galaxy NGC 4278 (Coma I Group) with peculiar velocities as extreme as -1000 km s⁻¹ (Karachentsev et al. 2011).

LV J1218+4655. This dwarf spiral (Sm) galaxy resides at a projected separation of 25' or 56 kpc from the massive spiral NGC 4258, with a distance of 7.83 ± 0.17 Mpc determined by Cepheids (Newman et al. 2001). Our distance to LV J1218+4655 of $D = 8.26 \pm 0.35$ Mpc is compatible with the status of LV J1218+4655 as a companion to NGC 4258.

Table 2. TRGB and distance measurements for the GO 14636 galaxies

Name	$F814W_{TRGB}$	$(F606W - F814W)_{TRGB}$	$E(B - V)$	μ_0	D , Mpc
BTS76	> 26.5		0.020	> 30.5	> 13
LV J1217+3231	> 26.5		0.010	> 30.5	> 13
LV J1218+4655	25.50 ± 0.07	$0.95^{+0.02}_{-0.05}$	0.017	29.59 ± 0.09	8.26 ± 0.35
KK144	24.82 ± 0.06	$0.99^{+0.03}_{-0.02}$	0.021	28.89 ± 0.08	$5.99^{+0.23}_{-0.22}$
NGC4455	25.06 ± 0.06	$1.13^{+0.02}_{-0.04}$	0.019	29.10 ± 0.09	6.61 ± 0.27
KK151	25.50 ± 0.04	1.03 ± 0.01	0.018	29.57 ± 0.07	8.20 ± 0.26
UGC07678	25.74 ± 0.04	1.16 ± 0.02	0.014	29.79 ± 0.07	9.08 ± 0.30
KK152	25.88 ± 0.05	$1.06^{+0.02}_{-0.01}$	0.016	29.95 ± 0.08	9.77 ± 0.35
KKSG29	25.92 ± 0.04	1.13 ± 0.02	0.026	29.96 ± 0.07	9.81 ± 0.31
NGC4618	25.42 ± 0.02	1.34 ± 0.01	0.019	29.42 ± 0.06	7.66 ± 0.22
LV J1243+4127	24.36 ± 0.09	$1.15^{+0.03}_{-0.02}$	0.015	28.41 ± 0.11	4.82 ± 0.24
NGC4656	25.43 ± 0.04	1.04 ± 0.01	0.011	29.51 ± 0.07	7.96 ± 0.25
IC3840	24.85 ± 0.06	1.05 ± 0.02	0.035	28.88 ± 0.08	5.99 ± 0.23
UGC08061	> 26.5		0.025	> 30.5	> 13
KK176	25.37 ± 0.06	1.08 ± 0.01	0.086	29.31 ± 0.09	7.28 ± 0.29
UGCA319	24.84 ± 0.03	1.01 ± 0.01	0.072	28.80 ± 0.07	5.75 ± 0.18
KK177	24.39 ± 0.04	1.10 ± 0.01	0.033	28.42 ± 0.07	4.82 ± 0.16
DDO161	$24.94^{+0.08}_{-0.04}$	1.07 ± 0.01	0.070	$28.90^{+0.10}_{-0.07}$	$6.03^{+0.29}_{-0.21}$
KDG218	> 26.5		0.040	> 30.5	> 13
NGC5068	$24.68^{+0.05}_{-0.06}$	$1.31^{+0.04}_{-0.02}$	0.091	$28.56^{+0.08}_{-0.09}$	$5.16^{+0.20}_{-0.21}$

KK144. This is an isolated low surface brightness (LSB) dIr galaxy with the high HI-mass-to-stellar-mass ratio $M_{HI}/M_* \sim 4$.

NGC 4455 = EVCC0711. This is a dwarf Sdm galaxy foreground to the Virgo Cluster. Together with UGC 7584 and KKH 80 it probably forms an association of dwarfs having a projected radius of 30 kpc and velocity dispersion of 20 km s^{-1} . We use in the distance measurement and show in the CMD only stars in the outer part of the galaxy. We selected the stars situated outside of the ellipse with the parameters: $X=2133$, $Y=2439$, $A=1705$, $B=675$, $PA=73.8$, where X, Y are the ellipse center pixel coordinates in the combined distortion-corrected mosaic F606W frame, A and B are major and minor axes in pix, and PA is position angle of the major axis in degrees.

MCG+07-26-012 = KK151. This Magellanic-type (Im) dwarf is likely a peripheral companion to NGC 4258, with a projected separation of 660 kpc and radial velocity difference of 27 km s^{-1} .

UGC 7678. This is a Im-type dwarf situated in vicinity of interacting pair NGC 4485/4490 ($D_{TRGB} = 8.91 \text{ Mpc}$, EDD) at a projected separation of 300 kpc. We use in the distance measurement and show in the CMD only stars in the outer part of the galaxy. We selected the stars situated outside of the ellipse with the parameters: $X=2286$, $Y=3138$, $A=900$, $B=579$, $PA=15$.

MCG+06-28-009 = KK152. This is a gas-rich dIr galaxy. Together with another dwarf galaxy AGC229089 and BCD galaxy NGC 4509 it probably forms a dwarf association with a projected radius of 90 kpc and velocity dispersion of 50 km s^{-1} .

KKSG29. This LSB dIr galaxy is a neighbor of NGC4594 ("Sombrero") at a projected separation of 1.3° or 220 kpc. However, their radial velocities differ by 332 km s^{-1} .

NGC 4618. This is a peculiar Sdm galaxy Arp 023 = VV073 with a distorted single-arm structure. Together with the nearby distorted Sdm galaxy NGC 4625 it forms a pair KPG349 with a projected separation of $9'$ and radial velocity difference of 70 km s^{-1} . Surprisingly, the TRGB distance to NGC 4618, $7.66 \pm 0.22 \text{ Mpc}$, differs significantly from that of NGC 4625, $11.75 \pm 0.59 \text{ Mpc}$ (McQuinn et al. 2017). We re-measured the TRGB-distance to NGC 4625 using its archival HST images and obtained a distance of $12.61 \pm 0.49 \text{ Mpc}$ in satisfactory agreement with the estimate by McQuinn et al. (2017). This is an astonishing, instructive case where a small angular separation between two galaxies, their small radial velocity difference, as well as apparent signs of interaction, do not ensure the spatial proximity of the galaxies. We use in the distance measurement and show in the CMD only stars in

the outer part of the galaxy. We selected the stars situated outside of the ellipse with the parameters: $X=2242$, $Y=1994$, $A=2000$, $B=1560$, $PA=40.7$.

LV J1243+4127. This is a gas-rich LSB dIr galaxy with $M_{HI} \simeq M_*$. Its projected separation from NGC 4736 (104 kpc) and small radial velocity difference, 92 km s^{-1} , allows us to assign it to the NGC 4736 suite.

NGC 4656. Hockey-stick-like Sm galaxy at a distance of $7.96 \pm 0.25 \text{ Mpc}$ is strongly distorted by interaction with the whale-like Sd galaxy NGC 4631 at $D = 7.38 \pm 0.23 \text{ Mpc}$ (Radburn-Smith et al. 2011). Both the galaxies are linked with a faint bridge (Karachentsev et al. 2015b). Near NGC 4656 on its northern edge there is an LSB companion NGC 4656UV detected in ultraviolet by GALEX. The galaxy is large and does not fit in the ACS field. We selected in our measurements the stars with $Y < 1560$ in the pixel coordinates of the combined distortion-corrected mosaic F606W frame.

IC 3840 = LSBC D575-01. A gas-rich dIr galaxy with an emission $H\alpha$ semi-ring structure on the northern side.

UGC 8061 = EVCC1253. This dIr galaxy lies 6.3° away from M87. Its CMD does not show the presence of RGB above $I = 26.5 \text{ mag}$, yielding a distance estimate $D > 13 \text{ Mpc}$. Apparently, UGC8061 belongs to the virial core of the Virgo Cluster.

KK176. This is an isolated LSB dIr galaxy with $M_{HI}/M_* = 2.3$. Its CMD has been presented by us earlier (Karachentsev et al. 2017b).

UGCA 319 and DDO161. These are two gas-rich dwarf galaxies constituting a physical pair. Their properties have been described recently by Karachentsev et al. (2017b). In the CMD and the distance measurement of DDO161 we selected the stars with $X < 1476$ or $X > 2772$ in the pixel coordinates of the combined distortion-corrected mosaic F606W frame.

KK177 = LSBC D575-03 = EVCC1290. This is a LSB dwarf spheroidal galaxy. Judging by its radial velocity of $V_{LG} = 228 \pm 60 \text{ km s}^{-1}$ (Kim et al. 2014) and distance of $D = 4.82 \pm 0.16 \text{ Mpc}$, KK177 is likely a satellite of NGC 4826 having $V_{LG} = 365 \text{ km s}^{-1}$ and $D = 4.41 \pm 0.20 \text{ (EDD)}$.

KDG218. This is an ultra-diffuse dwarf galaxy associated with a group around NGC 4958 at $D = 22$ Mpc or with the Virgo Southern Extension filament at $D = 16$ Mpc. Its properties and CMD has been discussed by [Karachentsev et al. \(2017a\)](#).

NGC 5068. The HST/ACS images are pointed on the SE periphery of this Scd galaxy to avoid crowded HII-regions. The CMD of NGC 5068 has been presented earlier ([Karachentsev et al. 2017b](#)). Here we selected in our measurements the stars with $Y < 2066$ in the pixel coordinates of the combined distortion-corrected mosaic F606W frame. Our estimate of TRGB distance to it, $D = 5.16 \pm 0.21$ Mpc, is well consistent with the PNLF distance $D = 5.45 \pm 0.52$ Mpc, derived by [Herrmann et al. \(2008\)](#). The galaxy is located on the outskirts of the group around NGC 5236 in Centaurus.

3. PATTERN OF INFALL IN FRONT OF VIRGO CLUSTER

New accurate distance measurements are used by us to clarify the radius of zero-velocity surface of the Virgo Cluster. To this end, we calculated Virgo-centric distances

$$D_{VC}^2 = D_g^2 + D_c^2 - 2D_g \times D_c \times \cos \Theta,$$

where D_g and D_c are distances to a galaxy and to the cluster center from observer, and Θ is the galaxy angular separation from M 87. The velocity of the galaxy with respect to the cluster center is determined by us in two models of "minor" and "major" attractors. The first case assumes that peculiar velocities of galaxies in the cluster vicinity are small in comparison with the regular Hubble flow, the second case implies that the infall velocity towards the cluster center prevails for most the galaxies over their tangential motions (see details in [Karachentsev & Nasonova \(2010\)](#)).

In the model of "minor" attractor the Virgo-centric velocity is

$$V_{VC} = V_g \times \cos \lambda - V_c \cos(\lambda + \Theta),$$

where

$$\tan \lambda = D_c \times \sin \Theta / (D_g - D_c \times \cos \Theta),$$

and in the case of "major" attractor it is

$$V_{VC} = [V_c \times \cos \Theta - V_g] / \cos \lambda.$$

Here, λ means the angle between the line of sight towards a galaxy and the line connecting the galaxy with the cluster center. This dichotomy is due to our ignorance of the full spatial velocity of the galaxy. The difference between the two models becomes negligible when a galaxy locates just in front of the cluster center ($\lambda \simeq 180^\circ$).

The terms V_{VC} and D_{VC} require the adoption of the distance and the mean velocity of the Virgo center. Following [Binggeli et al. \(1993\)](#); [Mei et al. \(2007\)](#), and [Kashibadze et al. \(2018, in preparation\)](#), we adopt: $V_c = 984 \text{ km s}^{-1}$, $D_c = 16.65 \text{ Mpc}$ that yields the peculiar velocity of the Virgo cluster (i.e. the infall velocity of the LG towards Virgo) as $V_{c,pec} = -231 \text{ km s}^{-1}$.

Among the galaxies with accurate distances in front of Virgo we selected 28 objects with a suitable angle $\lambda = [135 - 180^\circ]$. Pertinent data are collected in the [Table 3](#). The columns contain: (1) galaxy name, (2) supergalactic coordinates, (3) radial velocity in the LG rest frame, (4) galaxy distance from the MW, (5) angular separation from M 87, (6) Virgo-centric distance, (7) angular separation between the line of sight and the direction from the galaxy towards M 87, (8,9) Virgo-centric velocity in cases of the minor and the major attractor, respectively, (10) reference for the distance source. The galaxies are ranked by their distance D_{VC} in a range of 3 - 13 Mpc, hence avoiding the Virgo core. As can be seen, only eight of twenty of our targets satisfy the geometric condition $\lambda = 135 - 180^\circ$.

The distribution of 28 galaxies by distances and velocities relative to the Virgo Cluster center for the cases of minor and major attractors are presented in the upper and lower panels of the [Fig. 5](#). According to [Peñarrubia & Fattahi \(2017\)](#), the radial velocity profile around a spherically symmetrical overdensity can be expressed as

$$V_{VC}(D_{VC}) = H_0 \times D_{VC} - H_0 \times R_0 \times (R_0/D_{VC})^{1/2},$$

where R_0 is the radius of the zero-velocity surface to be found. The solid line in [Fig. 5](#) corresponds to this equation with parameters defined from the least squares method: $R_0 = 7.05 \text{ Mpc}$, $H_0 = 97 \text{ km s}^{-1} \text{ Mpc}^{-1}$, and dispersion $\sigma_V = 92 \text{ km s}^{-1}$ for the model of minor attractor, and $R_0 = 7.60 \text{ Mpc}$, $H_0 = 104 \text{ km s}^{-1} \text{ Mpc}^{-1}$, $\sigma_V = 105 \text{ km s}^{-1}$ for the case of major one.

Table 3. Galaxies with TRGB-distances in front of the Virgo Cluster.

Name	SGL SGB	V_{LG}	D	Θ	D_{VC}	λ	V_{VC}^{mi}	V_{VC}^{ma}	Ref
	deg	km s^{-1}	Mpc	deg	Mpc	deg	km s^{-1}	km s^{-1}	
(1)	(2)	(3)	(4)	(5)	(6)	(7)	(8)	(9)	(10)
UGC07512	112.36-6.46	1353	11.86	10	5.41	147	-225	-461	EDD
VCC2037	106.03+0.67	1032	9.64	4	7.08	170	-37	-52	EDD
IC3583	102.45-0.72	1024	9.51	2	7.15	176	-38	-41	EDD
GR34	99.00-3.36	1204	9.29	4	7.41	171	-209	-225	EDD
NGC4600	112.45-2.67	696	9.29	10	7.65	159	315	294	EDD
KK152	82.94+4.19	835	9.77	21	8.30	135	310	116	this work
NGC4517	114.82-5.32	972	8.36	12	8.67	156	76	-12	EDD
NGC4656	84.68+6.02	643	7.96	20	9.57	143	427	351	this work
NGC4631	84.21+5.74	581	7.35	20	10.09	145	476	417	EDD
NGC4455	92.75+0.19	588	6.61	10	10.22	163	415	398	this work
IC3840	95.26+5.02	510	5.97	11	10.84	164	490	477	this work
KK144	87.12+1.16	452	5.99	16	11.02	155	562	543	this work
AGC749241	90.11+3.65	418	5.62	14	11.28	159	587	575	McQuinn et al. (2014)
Arp211	77.94+6.41	484	6.14	26	11.48	140	586	520	EDD
KDG215	97.94+5.26	362	4.83	9	11.90	167	629	625	EDD
KK177	95.64+7.54	228	4.82	12	11.98	163	763	768	this work
UA319	133.53-2.93	549	5.75	31	12.06	135	564	419	this work
DDO133	84.65+3.58	320	4.88	19	12.15	153	690	682	EDD
DDO126	78.93+4.02	230	4.97	25	12.31	145	780	805	EDD
NGC4395	82.30+2.73	313	4.76	21	12.33	151	701	693	EDD
NGC4826	95.60+6.12	363	4.41	11	12.35	165	631	624	EDD
PGC038685	78.54+0.54	340	4.85	25	12.40	146	689	669	EDD
UGC07605	80.39+3.91	316	4.74	23	12.44	148	705	693	EDD

Table 3. Continued.

Name	SGL SGB	V_{LG}	D	Θ	D_{VC}	λ	V_{VC}^{mi}	V_{VC}^{ma}	Ref
	deg	km s^{-1}	Mpc	deg	Mpc	deg	km s^{-1}	km s^{-1}	
(1)	(2)	(3)	(4)	(5)	(6)	(7)	(8)	(9)	(10)
DDO127	78.92+4.31	290	4.72	25	12.53	146	731	727	EDD
LVJ1243+41	75.60+8.30	444	4.82	29	12.66	140	626	541	this work
IC3687	78.42+7.27	377	4.57	26	12.71	145	664	620	EDD
DDO154	90.12+6.89	354	4.04	16	12.81	159	649	634	EDD
NGC4244	77.72+2.40	257	4.31	26	12.90	156	760	760	EDD

To estimate the input of distance errors into the galaxy scatter on the Fig. 5 diagrams we adopt their typical distance error of 5%. As seen from the diagrams, the R_0 value is the most sensitive to positions of seven galaxies having $D_{VC} < 9$ Mpc. At their average distance from the Milky Way of 9.7 Mpc, the average scatter of Virgo-centric distances is 0.57 Mpc. This corresponds to the Virgo-centric velocity scatter of 78 km s^{-1} and 90 km s^{-1} for the cases of minor and major attractor, respectively. Consequently, we can say that the velocity dispersion on the panels of Fig. 5 is low and contributed mostly by galaxy distance errors. The cold Hubble flow around the Virgo Cluster may impose constraints on some models of cluster formation.

In the standard cosmological Λ CDM model, where Ω_m is the mean cosmic density of matter, G is the gravitational constant and H_0 the Hubble parameter, the relation between R_0 and the total mass of overdensity is

$$M_T = (\pi^2/8G) \times R_0^3 \times H_0^2/f^2(\Omega_m).$$

Here, the dimensionless parameter $f(\Omega_m)$ changes in the range from 1 to $2/3$ while varying Ω_m from 0 to 1. Taking the WMAP parameters: $\Omega_m = 0.24$, $\Omega_\lambda = 0.76$ and $H_0 = 73 \text{ km s}^{-1} \text{ Mpc}^{-1}$, we obtain the relation

$$(M_T/M_\odot)_{0.24} = 2.12 \times 10^{12} (R_0/\text{Mpc})^3$$

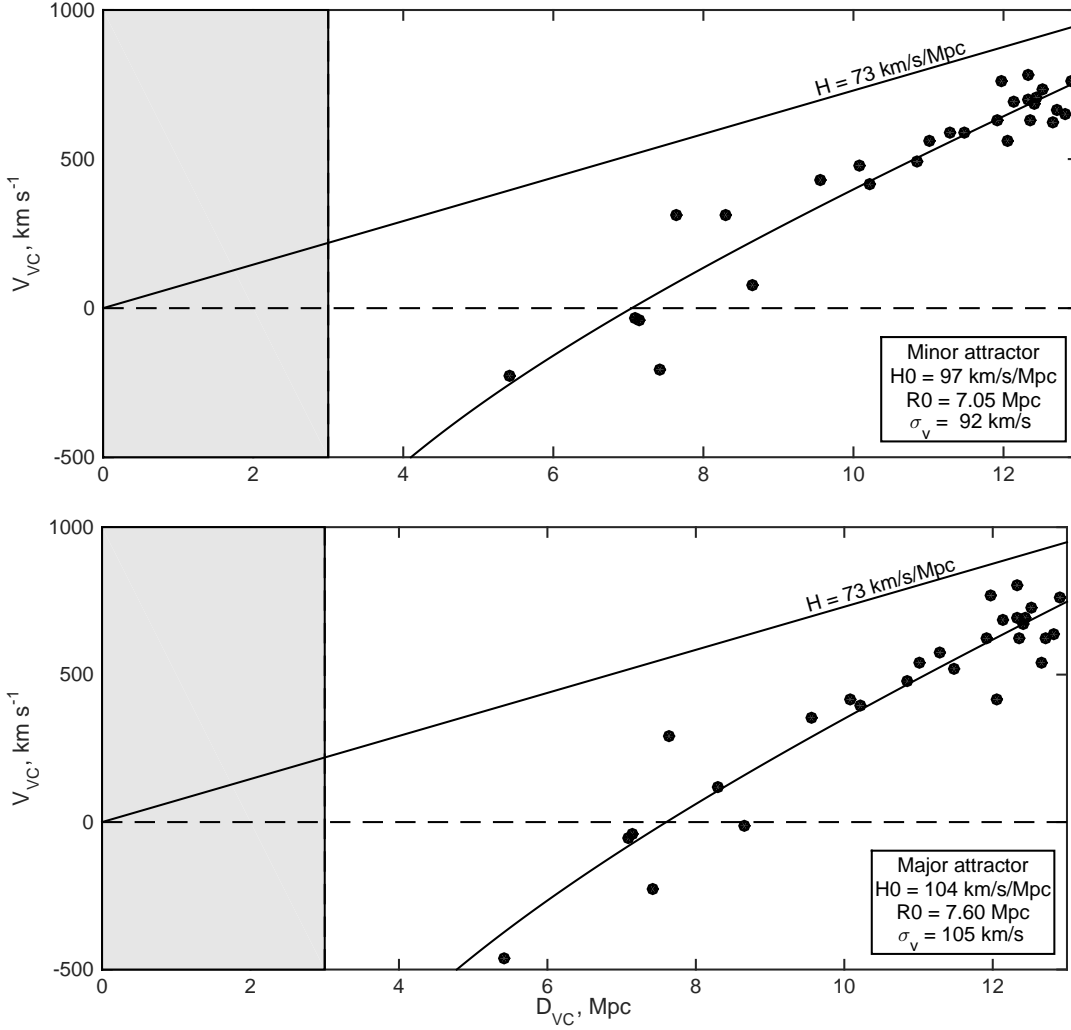


Figure 5. Hubble diagram "velocity - distance" in the Virgo Cluster frame. Upper and lower panels correspond to the cases of "minor" and "major" attractor, respectively. The area of virial motions is shaded.

. Accordingly, the radius $R_0 = 7.32 \pm 0.28 \text{ Mpc}$ yields the total mass estimate for the Virgo cluster $M_T = (8.31 \pm 0.94) \times 10^{14} M_\odot$. Under the Planck model parameters ($\Omega_m = 0.315, \Omega_\lambda = 0.685$ and $H_0 = 67.3 \text{ km s}^{-1} \text{ Mpc}^{-1}$), the total mass estimate drops to $M_T = (7.64 \pm 0.91) \times 10^{14} M_\odot$. This quantity derived from external galaxy motions agrees well with the internal virial mass estimates: $6.2 \times 10^{14} M_\odot$ (de Vaucouleurs 1960), $7.5 \times 10^{14} M_\odot$ (Tully & Shaya 1984), $7.2 \times 10^{14} M_\odot$ (Giraud 1999). The location of the turnaround radius and mass within it agree in detail with the values found by numerical action orbit reconstructions (Shaya et al. 2017) of $7.3 \pm 0.3 \text{ Mpc}$ and $8.3 \pm 0.3 \times 10^{14} M_\odot$.

4. CONCLUSIONS

The particular targets of these most recent observations with HST were chosen to clarify the situation regarding the transition to infall toward the cluster. The location of this transition provides an accurate estimate of the mass associated with the cluster out to the transition radius.

Of the 20 program targets, 16 distances less than 10 Mpc were successfully measured with characteristic accuracies of 5% using the TRGB methodology. The remaining four galaxies are inferred to lie beyond 13 Mpc, in spite of known velocities less than 500 km s^{-1} for three of them; one probably associated with the Virgo core and the other two adding to a curious anomaly associated with the Coma I Group.

The new measured distances add to pre-existing distances in an analysis of the velocity field in the proximity of the transition between Hubble expansion and Virgo infall. Within a reasonable range of assumptions, the Virgo turnaround radius is located at $R_0 = 7.3 \pm 0.3 \text{ Mpc}$ and the mass inside this radius is $8.3 \pm 0.9 \times 10^{14} M_\odot$. These values are in close agreement with measures from numerical action orbit reconstructions based on a much larger compendium of distances although lacking the 16 important new distances reported here.

This research is based on observations made with the NASA/ESA Hubble Space Telescope, program GO-14636, with data archive at the Space Telescope Science Institute. STScI is operated by the Association of Universities for Research in Astronomy, Inc. under NASA contract NAS 5-26555. The authors thank the anonymous referee for a thorough examination of the manuscript and for useful comments and suggestions to improve the text. Support for the program GO-14636 was provided by NASA through a grant from the Space Telescope Science Institute, which is operated by the Association of Universities for Research in Astronomy, Inc., under NASA contract NAS 5-26555. I.K. and L.M. acknowledge the support by the Russian Science Foundation grant 14-12-0096 and by RFBR grant 18-02-00005. The analysis of the galaxy distribution is supported by the Russian Science Foundation grant 14-12-0096. This research has made use of the NASA/IPAC Extragalactic Database (NED), which is operated by the Jet Propulsion Laboratory, California Institute of Tech-

nology, under contract with the National Aeronautics and Space Administration. We acknowledge the usage of the HyperLeda database (<http://leda.univ-lyon1.fr>). Help in the fitting Fig. 1 and Fig. 5 by Olga Kashibadze is greatly appreciated.

Facility: HST (ACS)

Software: DOLPHOT (Dolphin 2000), trgbtool (Makarov et al. 2006)

REFERENCES

- Aaronson, M., Huchra, J., Mould, J., Schechter, P. L., & Tully, R. B. 1982, *ApJ*, 258, 64
- Abazajian, K. N., Adelman-McCarthy, J. K., Agüeros, M. A., et al. 2009, *ApJS*, 182, 543
- Bahcall, N. A., & Kucler, A. 2014, *MNRAS*, 439, 2505
- Binggeli, B., Popescu, C. C., & Tammann, G. A. 1993, *A&AS*, 98, 275
- de Vaucouleurs, G. 1960, *ApJ*, 131, 585
- de Vaucouleurs, G., de Vaucouleurs, A., Corwin, Jr., H. G., et al. 1991, Third Reference Catalogue of Bright Galaxies. Volume I: Explanations and references. Volume II: Data for galaxies between 0^h and 12^h . Volume III: Data for galaxies between 12^h and 24^h .
- Dolphin, A. 2016, DOLPHOT: Stellar photometry, Astrophysics Source Code Library, , , ascl:1608.013
- Dolphin, A. E. 2000, *PASP*, 112, 1383
- Giraud, E. 1999, *ApJL*, 524, L15
- Herrmann, K. A., Ciardullo, R., Feldmeier, J. J., & Vinciguerra, M. 2008, *ApJ*, 683, 630
- Ibata, R. A., Lewis, G. F., Conn, A. R., et al. 2013, *Nature*, 493, 62
- Karachentsev, I. D. 2005, *AJ*, 129, 178
- Karachentsev, I. D., Kashibadze, O. G., Makarov, D. I., & Tully, R. B. 2009, *MNRAS*, 393, 1265
- Karachentsev, I. D., Makarova, L. N., Sharina, M. E., & Karachentseva, V. E. 2017a, *Astrophysical Bulletin*, 72, 376
- Karachentsev, I. D., Makarova, L. N., Tully, R. B., et al. 2017b, *MNRAS*, 469, L113
- Karachentsev, I. D., & Nasonova, O. G. 2010, *MNRAS*, 405, 1075
- Karachentsev, I. D., Nasonova, O. G., & Courtois, H. M. 2011, *ApJ*, 743, 123
- Karachentsev, I. D., Tully, R. B., Makarova, L. N., Makarov, D. I., & Rizzi, L. 2015a, *ApJ*, 805, 144
- Karachentsev, I. D., Tully, R. B., Wu, P.-F., Shaya, E. J., & Dolphin, A. E. 2014, *ApJ*, 782, 4
- Karachentsev, I. D., Riepe, P., Zilch, T., et al. 2015b, *Astrophysical Bulletin*, 70, 379
- Kashibadze, O. G., & Karachentsev, I. D. 2018, *A&A*, 609, A11

- Kim, S., Rey, S.-C., Jerjen, H., et al. 2014, *ApJS*, 215, 22
- Makarov, D., Makarova, L., Rizzi, L., et al. 2006, *AJ*, 132, 2729
- Makarov, D., Prugniel, P., Terekhova, N., Courtois, H., & Vauglin, I. 2014, *A&A*, 570, A13
- Mandelbaum, R., Seljak, U., Kauffmann, G., Hirata, C. M., & Brinkmann, J. 2006, *MNRAS*, 368, 715
- McQuinn, K. B. W., Skillman, E. D., Dolphin, A. E., Berg, D., & Kennicutt, R. 2017, *AJ*, 154, 51
- McQuinn, K. B. W., Cannon, J. M., Dolphin, A. E., et al. 2014, *ApJ*, 785, 3
- Mei, S., Blakeslee, J. P., Côté, P., et al. 2007, *ApJ*, 655, 144
- Newman, J. A., Ferrarese, L., Stetson, P. B., et al. 2001, *ApJ*, 553, 562
- Peñarrubia, J., & Fattahi, A. 2017, *MNRAS*, 468, 1300
- Peebles, P. J. E. 1989, *ApJL*, 344, L53
- Peebles, P. J. E., Phelps, S. D., Shaya, E. J., & Tully, R. B. 2001, *ApJ*, 554, 104
- Peirani, S., & de Freitas Pacheco, J. A. 2008, *A&A*, 488, 845
- Radburn-Smith, D. J., de Jong, R. S., Seth, A. C., et al. 2011, *ApJS*, 195, 18
- Rizzi, L., Tully, R. B., Makarov, D., et al. 2007, *ApJ*, 661, 815
- Rizzi, L., Tully, R. B., Shaya, E. J., Kourkchi, E., & Karachentsev, I. D. 2017, *ApJ*, 835, 78
- Schlafly, E. F., & Finkbeiner, D. P. 2011, *ApJ*, 737, 103
- Shaya, E. J., Peebles, P. J. E., & Tully, R. B. 1995, *ApJ*, 454, 15
- Shaya, E. J., & Tully, R. B. 2013, *MNRAS*, 436, 2096
- Shaya, E. J., Tully, R. B., Hoffman, Y., & Pomarède, D. 2017, *ApJ*, 850, 207
- Tully, R. B. 2015, *AJ*, 149, 54
- Tully, R. B., & Fisher, J. R. 1977, *A&A*, 54, 661
- . 1987, *Nearby galaxies Atlas*
- Tully, R. B., Libeskind, N. I., Karachentsev, I. D., et al. 2015, *ApJL*, 802, L25
- Tully, R. B., & Shaya, E. J. 1984, *ApJ*, 281, 31
- Tully, R. B., Shaya, E. J., Karachentsev, I. D., et al. 2008, *ApJ*, 676, 184
- Tully, R. B., Rizzi, L., Dolphin, A. E., et al. 2006, *AJ*, 132, 729
- van Uiter, E., Hoekstra, H., Velandier, M., et al. 2011, *A&A*, 534, A14
- Ziparo, F., Smith, G. P., Mulroy, S. L., et al. 2016, *A&A*, 592, A9